Article

Research on the Magnetic Field Distribution in Drum-Type Eddy Current Separation

Youdong Jia , MingJiang Jiang , Jianxiong Liu * , Sibo Yao , Lei Wang , Jiaxing Zeng , Xiangming Wan

Posted Date: 5 July 2024

doi: 10.20944/preprints202407.0466.v1

Keywords: Eddy current separation; Permanent magnet; Separation of nonferrous metals; Recovery of end-of- life vehicles

Article

Research on the Magnetic Field Distribution of Eddy Current Separator's Magnetic Drum Based on Analytical Calculation and Numerical Analysis

Jia Youdong [1,4], Jiang Mingjiang [1], Liu Jianxiong [1,*], Yao Sibo [2,3], Wang Lei [4],Zeng Jiaxing [1] and Wan Xiangming [1]

[1] Faculty of Mechanical and Electrical Engineering,Kunming University of Science and Technology,Kunming 650500
[2] School of Mechanical Engineering & Automation, Northeastern University, Shenyang 110819
[3] Key Laboratory of Vibration and Control of Aero-Propulsion System, Ministry of Education, Shenyang 110819
[4] Faculty of Mechanical and Electrical Engineering,Kunming University,Kunming 650214
* Correspondence: jxlkmust@163.com

Abstract: As the number of end-of-life vehicles continues to grow, the field of separation technology for broken copper and aluminium parts of end-of-life vehicles has emerged as a significant area of research. As a key technology for the separation of non-magnetic non-ferrous metals, such as copper and aluminium, eddy current separation can achieve efficient separation of non-magnetic non-ferrous metals according to their differing conductivity and density. Nevertheless, further research is required in the separation of large-scale broken copper and aluminium parts of end-of-life vehicles. This paper presents a novel magnetic roller model comprising circumferential and axial periodic arrangements of permanent magnets. A single permanent magnet was constructed as an equivalent current model, and the magnetic scalar potential equations were solved using simulation tools. This allowed the distribution of the magnetic field outside the magnetic roller to be studied. The results demonstrate that the novel permanent magnet array magnetic roller can enhance the magnetic field intensity and action distance of the external magnetic field, which is more conducive to the separation of large-scale broken copper and aluminium parts of scrap cars. The findings of this research provide a theoretical foundation for the separation of scrap car broken copper and aluminium parts

Keywords: Eddy current separation; Permanent magnet;Separation of nonferrous metals;Recovery of end-of- life vehicles

1. Introduction

In 2020, China's automobile ownership will exceed 270 million, and theoretically, the number of end-of-life automobiles should reach 18.51 million [1–3], and based on an average end-of-life weight of 1.28 tons per automobile, the end-of-life automobiles in that year should amount to 23.69 million tons, which includes 16.58 million tons of iron and steel, 1.43 million tons of non-ferrous metals such as copper and aluminium and 4.27 million tons of waste plastics and rubber [4]. However, due to the relative lag in the development of theories, technologies and equipment for recycling end-of-life automobiles, only 2.03 million of these vehicles have been recycled, with a recycling rate as low as 11%. The effective separation and recycling of magnetic materials in end-of-life automobiles can be well realized by crushing and magnetic sorting [5–8], but the separation of complex, heterogeneous, thin-walled copper and aluminum and other non-magnetic metal materials has not been solved so far [9], and as the basic materials for the development of the national economy, the secondary comprehensive utilization of these materials is of great practical significance.

As the basic means of separating non-magnetic non-ferrous metal materials such as copper and aluminum, eddy current separation theory, technology and equipment still need to be further studied

 doi:10.20944/preprints202407.0466.v1

and improved. 1982 KERCHER et al. [10] applied the eddy current separation technology to the separation of aluminum and copper in the processing of steel scrap and conducted experimental evaluation of eddy current separation capacity. 1986 VANDERVALK et al. [11] proposed a specific method to optimize the magnetic roll structure of the separation system and developed a rotating disc type eddy current separator using this method. 1991 FLETCHER et al. [12] researched and developed a rotating disc type eddy current separator, developed a single-field boundary eddy current separator and deduced the theoretical trajectories of particles of both circular and rectangular shaped models passing through this device.

In 1992, NORRGRAN et al [13] arranged NdFeB permanent magnets regularly on the surface of a high-speed rotating cylinder, and realized the separation of nonferrous metals in automobile crushed materials with particle size below 6.4 mm. In 1997, REM et al [14,15] proposed a mathematical model for the study of particle trajectory in the process of eddy-current separation, and set up a computer simulation model of the separation mechanism of the rotary-drum eddy-current separator, and experimentally analyzed and tested the theoretical trajectories of particles passing through the device. A computer simulation model of the separation mechanism of drum eddy current sorting was established, and the model was verified through experiments.

In 1998, ZHANG et al [16,17] used their self-developed powerful eddy current sorter to separate and recover aluminum from computer crushed materials, and obtained a purity of 85% pure aluminum metal, and in the same year, they also used ECSIM simulation tool to simulate numerically the trajectory of the aluminum particles in the double-drum eddy current sorter.In 2002, SCHLETT et al [18]researched and developed a new type of eddy current sorter for separating nonferrous metals from the mixture containing dielectric particles. In 2002, LUNGU et al [19,20] developed the Inclined Drum Eddy Current Separator (IDECS) for improving the separation effect, and in 2003, the Single Disk Eddy Current Separator (SDECS) was developed. In 2012, ROY et al [21] investigated the applicability of eddy current separation technology for fine particle (1mm) e-waste. 2013, RAHMAN et al [22] installed sensors in an eddy current sorter to accurately measure the purity of a stream of metal particles to be sorted, and experimentally investigated the effect of the magnetic roll axial deflection on the purity of the metal in the stream. In 2016, AMIR et al [23] developed a low-cost domestic eddy current sorter. Domestic research on the theory, technology and equipment of eddy current separation is relatively late. 2005 Wang Quanqiang et al [24] studied the separation method of copper and aluminum particles based on the difference of conductivity and density. 2011 Ruan Jujun et al [25] studied the recycling technology of end-of-life toner cartridges, and established a new mathematical model of eddy current force.In 2015, Yu Dunsheng et al [26]reviewed the current situation of recycling of end-of-life vehicles, emphasized the importance of crushing and separation, and looked forward to the prospect and development trend of eddy current separation technology in the recycling of end-of-life vehicles. In 2016, Li Jia et al. [27] established a mathematical model of the trajectory of copper and aluminum particles in the eddy current separation device, and analyzed the optimal separation conditions under different feeding speeds, particle diameters, and rotational speeds of the magnetic rollers. 2018, Li Jianbo et al. [28] used the eddy current separation technology to realize the effective separation and recycling of positive and negative electrode materials, copper foils, aluminum foils, and septums of lithium-ion battery cores. 2020, Wei Honggang et al. Wei Honggang et al [29] simulated and analyzed the process of eddy current separation of nonferrous metal particles, derived the formula of magnetic field strength on the surface of magnetic rollers, and established the corresponding kinematics equations. 2020 Ye Fangping et al [30]developed a medium-sized eddy current sorter for nonferrous metal recovery from solid waste. 2020 Chen Stalin et al [31] developed two types of magnetic field strengths and their spatial distribution based on the magnetic field model of a single permanent magnet. Based on the magnetic field model of a single permanent magnet, Chen Lin et al. gave the magnetic field strength and its spatial distribution law of two arrangements, indicating that the Halbach arrangement is more suitable for the separation of large-size copper and aluminum parts than the N-S-N arrangement. With the development of samarium cobalt and neodymium-iron-boron (NdFeB) and other new rare-earth permanent magnetic materials, the development of permanent magnetic eddy current separation theory, technology and

Preprints.org (www.preprints.org) | NOT PEER-REVIEWED | Posted: 5 July 2024 doi:10.20944/preprints202407.0466.v1

equipment is in the ascendant, and it is becoming an important development direction of eddy current separation technology [32].

In summary, the current domestic and foreign research on eddy current separation is mainly focused on the separation of fine non-ferrous metal materials, eddy current force modeling, multi-factor coupling to improve the separation effect, research and development of new equipment, as well as through the introduction of a new type of "computer-sensor" control device, real-time on-line monitoring and intelligent control of the separation system and process. Monitoring and intelligent control of the separation system and process in real time online. However, the end-of-life automobile crushing products in the size and quality of relatively large copper and aluminum parts of the separation of theory, technology and equipment are still in need of further research.In this paper, a new permanent magnet roll model is constructed with a specific arrangement of permanent magnets: a single permanent magnet is magnetized in parallel, with every four permanent magnets in the axial direction and every six permanent magnets in the circumferential direction. By constructing an equivalent current model of a single permanent magnet and utilizing finite element simulation software, the distribution pattern of the magnetic field outside the roll was investigated, and the optimal geometric parameters of the roll were determined in order to achieve good separation results.

2. New Permanent Magnet Roller Model Structure

The development of rare-earth permanent magnetic materials and technologies has brought new opportunities for the theory, technology and equipment of permanent magnet eddy current separation. In this study, a new type of permanent magnet array magnetic roller model is constructed through a specific arrangement of permanent magnets, as shown in Figure 1. This arrangement differs from previous models in that the permanent magnets are not only arranged in the circumferential direction with alternating cycles, but also in the axial direction with alternating cycles. The model is characterised by four main aspects: all permanent magnets are magnetised in parallel; single permanent magnets are arranged in different directions; permanent magnets with radial dimensions R_1 and R_2, circumferential dimensions α_1 and α_2, and axial dimensions L_1 and L_2 are arranged in alternating cycles.

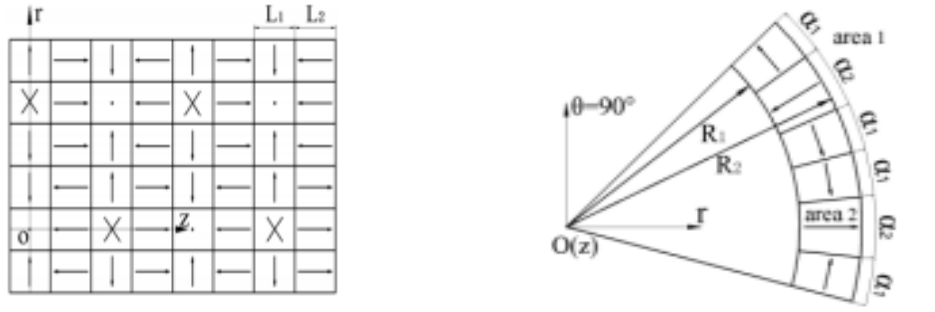

(**a**) Axial arrangement (**b**) Circumferential arrangement

Figure 1. New permanent magnet array model.

3. Results

The rolls are arranged on the surface of the rolls in alternating cycles. In the circumferential direction, one cycle is dedicated to each of the six permanent magnets, while in the axial direction, one cycle is allotted to each of the four permanent magnets.

By modifying the geometry of the permanent magnets in terms of diameter, circumference and axial direction, the rolls are optimized to determine the most suitable physical and sorting parameters, with the objectives of increasing the flux density at the axial peaks and valleys of the rolls' magnetic field and improving the separation of non-ferrous metal lumps.

 doi:10.20944/preprints202407.0466.v1

3. Research on the Magnetic Field of Magnetic Rollers Based on Circulation

A study of the magnetic field of magnetic rollers based on ring current. In order to obtain the change law of magnetic field strength of permanent magnet rollers with alternating circumferential-axial periodic arrangement, it is first necessary to study the magnetic field characteristics of radial, circumferential, and axial unidirectional magnetized single permanent magnets. From the Ampere molecular current theorem, it is possible to derive a parallel magnetized permanent magnet equivalent current model.

The single radial magnetized permanent magnet equivalent current model, as illustrated in Figure 2, represents the total equivalent current.

$$\overrightarrow{I_r} = \overrightarrow{J_r}(R_2 - R_1) \tag{1}$$

In the formula: for a single radial magnetized permanent magnet radial unit length ring current density; R_1, R_2 for a radial size of a single permanent magnet.

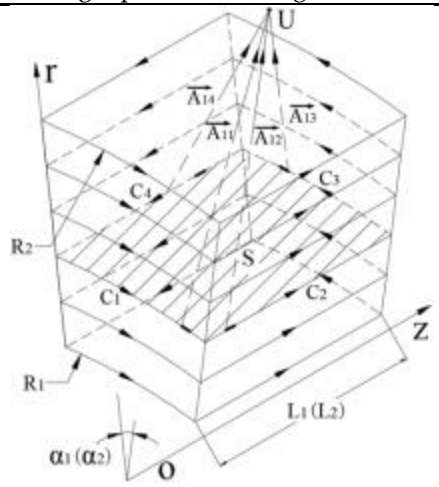

Figure 6. Model of outer end region of magnetic roller

From the planar current-carrying coil magnetic moment model, the total magnetic moment m inside a single radially magnetized permanent magnet $\vec{m}$ is:

$$\vec{m} = \sum \vec{p_m} = | \vec{I_r} | \vec{Se} \tag{2}$$

where: the vector $\vec{p_m}$ is the magnetic moment of a single toroidal coil: S is the area of the mid-section of a single permanent magnet orthogonal to the r-axis; $\vec{e}$ is the unit vector in a right-handed helical relationship with the current direction.

This results in a magnetization strength of:

$$\vec{M} = \frac{\vec{m}}{\Delta V} = \frac{|\overrightarrow{J_r}|(R_2 - R_1)S\vec{e}}{S(R_2 - R_1)} = |\overrightarrow{J_r}|\vec{e} \tag{3}$$

where: $\vec{M}$ is the magnetization intensity of a single radially magnetized permanent magnet, which is a constant vector for uniform magnetization; ΔV is the volume of a single permanent magnet.

Taking the ring current path as $C_1C_2C_3C_4$ in Figure 2, the current on the radial dimension dr ring segment is:

$$\vec{I} = \vec{J_r} dr \tag{4}$$

rom the Biot-Saval law, the current element idc at any point in space $U(r_u, \theta_u, z_u)$ at any point in space produces a magnetic flux density of:

Preprints.org (www.preprints.org) | NOT PEER-REVIEWED | Posted: 5 July 2024 doi:10.20944/preprints202407.0466.v1

$$d\vec{B} = \frac{\mu_0}{4\pi} \cdot \frac{|\vec{I}|\overrightarrow{dc} \times \vec{A}}{|\vec{A}|^3} \tag{5}$$

Wherwhere: μ_0 is the vacuum permeability; the vector $\overrightarrow{dc}$ is the circulating path microlinear element; the vector $\vec{A}$ is the vectorial diameter of the taken linear element to the point U.

Consider the relationship between the right-angle coordinate system and the column coordinate system:

$$\begin{aligned} x_1 &= r\cos\theta \\ y_1 &= r\sin\theta \\ z_1 &= z \end{aligned} \tag{6}$$

The flux density B at the point $U(r_u, \theta_u, z_u)$ outside a single radially magnetized permanent magnet can be expressed as:

$$\begin{aligned} \overrightarrow{B_1} = \{ & \int_{R_1}^{R_2} \int_0^{\alpha_1} r d\theta dr \left|\bar{A}_{11}\right|^{-3} [z_u \cos\theta \vec{i} + z_u \sin\theta \vec{j} + (\sin\theta \cdot \\ & (r\sin\theta - r_u \sin\theta_u) + \cos\theta (r\cos\theta - r_u \cos\theta_u))\vec{k}] + \\ & \int_{R_1}^{R_2} \int_0^{\alpha_1} r d\theta dr |\overrightarrow{A_{13}}|^{-3} [(L_1 - z_u)\cos\theta \vec{i} + (L_1 - z_u)\sin\theta \vec{j} \\ & + (\sin\theta (r_u \sin\theta_u - r\sin\theta) + \cos\theta (r_u \cos\theta_u - r\cos\theta)) \cdot \\ & \vec{k}] + \int_{R_1}^{R_2} \int_0^{L_1} dz dr \left|\bar{A}_{12}\right|^{-3} [(r\sin\alpha_1 - r_u \sin\theta_u)\vec{i} - (r\cos\alpha_1 \\ & - r_u \cos\theta_u)\vec{j}] + \int_{R_1}^{R_2} \int_0^{L_1} dz dr |\overrightarrow{A_{14}}|^{-3} [r_u \sin\theta_u \vec{i} - (r_u \cos\theta_u \\ & |-r)\vec{j}]\} \frac{\mu_0 |\vec{M}|}{4\pi} \end{aligned} \tag{7}$$

Where: i,i, j, k are the unit vectors of parallel axes in the Cartesian coordinate system;

$$\begin{aligned} \bar{A}_{11} &= (r_u \cos\theta_u - r\cos\theta, r_u \sin\theta_u - r\sin\theta, z_u) \\ \bar{A}_{12} &= (r_u \cos\theta_u - r\cos\alpha_1, r_u \sin\theta_u - r\sin\alpha_1, z_u - z) \\ \bar{A}_{13} &= (r_u \cos\theta_u - r\cos\theta, r_u \sin\theta_u - r\sin\theta, z_u - L_1) \\ \bar{A}_{14} &= (r_u \cos\theta_u - r, r_u \sin\theta_u, z_u - z) \end{aligned} \tag{8}$$

Similarly, the equivalent current model and its external flux density at $U(r_u,\theta_u,z_u)$ shown in Figure 3 for a single circumferentially magnetized permanent magnet can be obtained.

The equivalent current model of a single circumferentially magnetized permanent magnet and its external flux density at the point $U(r_u,\theta_u,z_u)$ are shown in Figure 3:

Preprints.org (www.preprints.org) | NOT PEER-REVIEWED | Posted: 5 July 2024 doi:10.20944/preprints202407.0466.v1

$$\begin{aligned}\bar{B}_2 = \{&\int_{R_1}^{R_2}\int_0^{\alpha_1} R_1 d\theta dr\left|\overrightarrow{A_{21}}\right|^{-3}[z_u\cos\theta\vec{j} - z_u\sin\theta\vec{i} + (\cos\theta\cdot(r\sin\theta - r_u\sin\theta_u) - (r\cos\theta \\ &- r_u\cos\theta_u)\sin\theta)\vec{k}] + \\ &\int_{R_1}^{R_2}\int_0^{\alpha_1} R_1 d\theta dr\left|\bar{A}_{23}\right|^{-3}[(z_u - L_1)\sin\theta\vec{i} - (z_u - L_1)\cos\theta\vec{j} \\ &+((r_u\sin\theta_u - r\sin\theta)\cos\theta - (r_u\cos\theta_u - r\cos\theta)\sin\theta)\cdot \\ &\vec{k}] + \int_0^{\alpha_1}\int_0^{L_1} R_1 d\theta dz\left|\bar{A}_{22}\right|^{-3}[(R_1\sin\theta - r_u\sin\theta_u)\vec{i} + (r_u\cos\theta_u \\ &-R_1\cos\theta)\vec{j}] + \int_0^{\alpha_1}\int_0^{L_1} R_2 d\theta dz\left|\bar{A}_{24}\right|^{-3}[(r_u\sin\theta_u - R_2\sin\theta)\vec{i} \\ &-(r_u\cos\theta_u - R_2\cos\theta)\vec{j}]\}\frac{\mu_0|\bar{M}|}{4\pi}\end{aligned} \tag{9}$$

In the formula: A_{21},A_{22},A_{23},A_{24} are:

$$\begin{aligned}\bar{A}_{21} &= (r_u\cos\theta_u - r\cos\theta, r_u\sin\theta_u - r\sin\theta, z_u) \\ \bar{A}_{22} &= (r_u\cos\theta_u - R_1\cos\theta, r_u\sin\theta_u - R_1\sin\theta, z_u - z) \\ \bar{A}_{23} &= (r_u\cos\theta_u - r\cos\theta, r_u\sin\theta_u - r\sin\theta, z_u - L_1) \\ \bar{A}_{24} &= (r_u\cos\theta_u - R_2\cos\theta, r_u\sin\theta_u - R_2\sin\theta, z_u - z)\end{aligned} \tag{10}$$

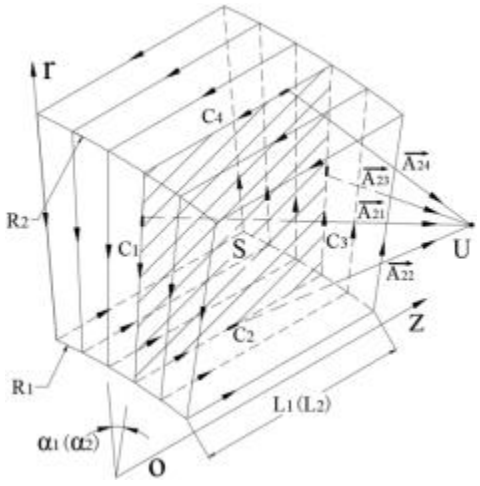

Figure 3. Equivalent current model of circumferential magnetized permanent magnet.

Similarly, the equivalent current model and its external flux density at $U(r_u, \theta_u, z_u)$ shown in Figure 4 for a single axially magnetized permanent magnet can be obtained.

The equivalent current model of a single axially charged permanent magnet shown in Figure 4 and its external flux density at $U(r_u, \theta_u, z_u)$ can be obtained.

$$\begin{aligned}\bar{B}_3 = \{&\int_{R_1}^{R_2}\int_0^{L_1} dzdr\left|\bar{A}_{31}\right|^{-3}[(z - z_u)\vec{j} + r_u\sin\theta_u\vec{k}] + \\ &\int_{R_1}^{R_2}\int_0^{L_1} dzdr\left|\bar{A}_{32}\right|^{-3}[\sin\alpha_1(z - z_u)\vec{i} + \cos\alpha_1(z_u - z)\vec{j}\end{aligned} \tag{11}$$

Preprints.org (www.preprints.org) | NOT PEER-REVIEWED | Posted: 5 July 2024 doi:10.20944/preprints202407.0466.v1

$$+(\cos\alpha_1(r\sin\alpha_1 - r_u\sin\theta_u) + (r_u\cos\theta_u - r\cos\alpha_1)\cdot\sin\alpha_1)\vec{k}] + \int_0^{L_1}\int_0^{\alpha_1} R_1 dz d\theta \left|\overrightarrow{A_{32}}\right|^{-3}[\cos\theta(z - z_u)\vec{i} -$$

$$\sin\theta(z_u - z)j + ((r_u\sin\theta_u - R_1\sin\theta)\sin\theta + (r_u\cos\theta_u - R_1\cos\theta)\cos\theta)\vec{k}] + \int_0^{L_1}\int_0^{\alpha_1} R_2 dz d\theta \left|\bar{A}_{34}\right|^3 [\cos\theta(z_u - z)\vec{i} + \sin\theta(z_u - z)\vec{j} + ((R_2\sin\theta - r_u\sin\theta_u)\sin\theta - (r_u\cos\theta_u - R_2\cos\theta)\cos\theta)\vec{k}]\}\frac{\mu_0 |\vec{M}|}{4\pi}$$

Formula: A_{31}, A_{32}, A_{33}, A_{34}

$$\begin{aligned}
\bar{A}_{31} &= (r_u\cos\theta_u - r, r_u\sin\theta_u, z_u - z)\\
\bar{A}_{32} &= (r_u\cos\theta_u - R_1\cos\theta, r_u\sin\theta_u - R_1\sin\theta, z_u - z)\\
\bar{A}_{33} &= (r_u\cos\theta_u - r\cos\alpha_1, r_u\sin\theta_u - r\sin\alpha_1, z_u - z)\\
\bar{A}_{34} &= (r_u\cos\theta_u - R_2\cos\theta, r_u\sin\theta_u - R_2\sin\theta, z_u - z)
\end{aligned} \tag{12}$$

Based on the construction of the equivalent current model of a single permanent magnet with different magnetizing directions and the calculation of the equivalent current, the characteristics of the external magnetic field of a single magnetized permanent magnet can be calculated, while the magnetic field of the external area of the magnetic roll can be regarded as the result of the joint action and contribution of multiple single permanent magnets with different magnetizing directions, except that the boundary conditions of the end areas on both sides of the roll are different from those of the non-end areas, which determines the characteristics of the magnetic field of the external area of the magnetic roll.

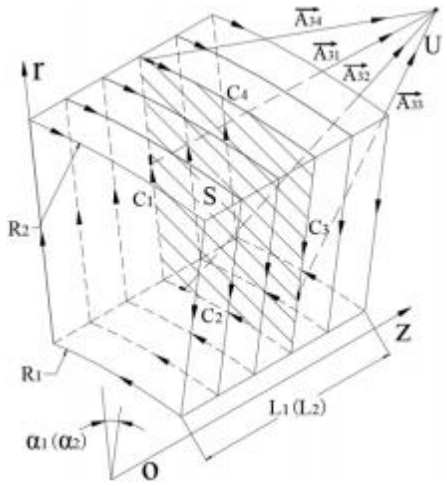

Figure 4. Equivalent current model of axially magnetized perma- nent magnet.

As shown in Figure 5, without loss of generality, the flux density at any point $V(r_v, \theta_v, z_v)$ in the non-end region outside the roll is the result of the combined contribution of nine single permanent magnets in the neighboring region with defined magnetization directions the flux density at point V is:

$$\begin{aligned}
\bar{B}_{v1} = {} & \overrightarrow{B_2}(r_v, \theta_v, z_v) + \overrightarrow{B_1}(r_v, \theta_v - \alpha_1, z_v) - \overrightarrow{B_2}(r_v, \theta_v - 2\alpha_1, z_v)\\
& -\vec{B}_3(r_v, \theta_v, z_v - L_1) - \vec{B}_3(r_v, \theta_v - \alpha_1, z_v - L_1) -\\
& \overrightarrow{B_3}(r_v, \theta_v - 2\alpha_1, z_v - L_1) - \overrightarrow{B_2}(r_v, \theta_v, z_v - 2L_1)\\
& -\vec{B}_1(r_v, \theta_v - \alpha_1, z_v - 2L_1) + \vec{B}_2(r_v, \theta_v - 2\alpha_1, z_v - 2L_1)
\end{aligned} \tag{13}$$

Preprints.org (www.preprints.org) | NOT PEER-REVIEWED | Posted: 5 July 2024 doi:10.20944/preprints202407.0466.v1

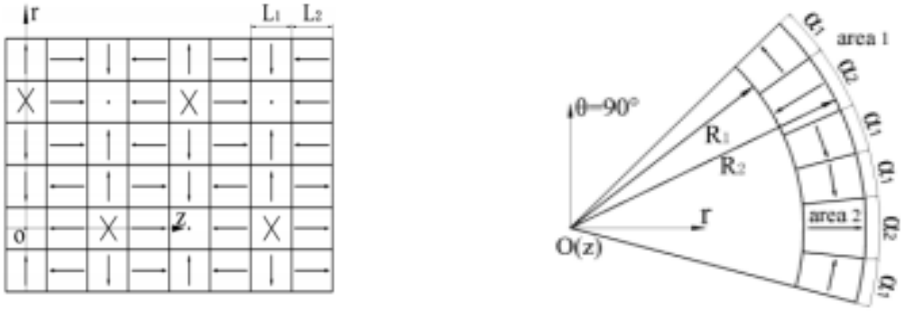

Figure 5. Model of non end region outside magnetic roller.

This section

As shown in Figure 6, similarly, the flux density at any point V(r_v,θ_v,z_v) in the area of the outer end of the roll is the result of the combined contribution of six single permanent magnets in the neighboring area with a defined magnetizing direction. The flux density at point V is:

Figure 6. Model of outer end region of magnetic roller.

3.1. Subse

$$\begin{aligned}\vec{B}_{v2} = {} & \overrightarrow{B_2}(r_v,\theta_v,z_v)+\overrightarrow{B_1}(r_v,\theta_v-\alpha_1,z_v)-\overrightarrow{B_2}(r_v,\theta_v-2\alpha_1,z_v)\\ & -\vec{B}_2(r_v,\theta_v,z_v-L_1)-\vec{B}_2(r_v,\theta_v-\alpha_1,z_v-L_1)\\ & -\overrightarrow{B_2}(r_v,\theta_v-2\alpha_1,z_v-L_1)\end{aligned} \tag{14}$$

So far can be calculated to get the magnetic roller external magnetic field change rule.

4. Magnetic Roll Magnetic Field Study Based on Magnetic Scalar Potentials

In order to further understand the pattern of changes in the magnetic field of the new arrangement of permanent magnet rolls, it is assumed that the magnetization intensity of a single permanent magnet magnet magnetized in parallel in any direction is equal, that the relative permeability of the materials used in the support rolls of the permanent magnets and the connectors between the permanent magnets and the support rolls is infinite, and that there are no gaps between the permanent magnets or between the permanent magnets and the support rolls.

The dispersion of the passive field is 0 by Gauss's law of magnetism, so it is within the magnetic field of the magnetic rollers:

$$\nabla \cdot \vec{B} = 0 \tag{15}$$

Where: B-⟶ is the magnetic flux density; $\nabla \cdot B$ is the dispersion of B-⟶. The magnetic field strength is expressed by the magnetic scalar potential as:

$$\vec{H} = -\nabla\varphi = -\frac{\partial\varphi}{\partial r}\overrightarrow{e_r} - \frac{1}{r}\frac{\partial\varphi}{\partial\theta}\overrightarrow{e_\theta} - \frac{\partial\varphi}{\partial z}\overrightarrow{e_z} \tag{16}$$

 doi:10.20944/preprints202407.0466.v1

Where: H is the magnetic field strength; ϕ is the magnetic scalar potential; $\nabla\phi$ is the gradient of ϕ; $\vec{e_r}, \vec{e_\theta}, \vec{e_z}$ are the unit vectors parallel to the coordinate axes in the cylindrical coordinate system.

Regions 1 and 2 are the external region of the magnetic roll surface and the internal region of the permanent magnet, respectively, as shown in Figure 1b. The flux densities B and magnetic field strengths H in areas 1 and 2 satisfy the relationship:

$$\begin{aligned} \vec{B_1} &= \mu_1 \vec{H_1} \\ \vec{B_2} &= \mu_2(\vec{H_2} + \vec{M}) \end{aligned} \tag{17}$$

where: B1, B2 are the flux densities in regions 1 and 2; H_1, H_2 are the magnetic field strengths in regions 1 and 2; M is the magnetization strength of permanent magnets; μ_1, μ_2 are the permeabilities in air and permanent magnets.

Substituting Equations (15) and (16) into (14), the magnetic scalar potentials in regions 1 and 2 are satisfied:

$$\begin{cases} \dfrac{\partial^2\varphi_1}{\partial r^2} + \dfrac{1}{r}\dfrac{\partial\varphi_1}{\partial r} + \dfrac{1}{r^2}\dfrac{\partial^2\varphi_1}{\partial\theta^2} + \dfrac{\partial^2\varphi_1}{\partial z^2} = 0 \\ \dfrac{\partial^2\varphi_2}{\partial r^2} + \dfrac{1}{r}\dfrac{\partial\varphi_2}{\partial r} + \dfrac{1}{r^2}\dfrac{\partial^2\varphi_2}{\partial\theta^2} + \dfrac{\partial^2\varphi_2}{\partial z^2} = \nabla\cdot\vec{M} \end{cases} \tag{18}$$

Where: φ_1, φ_2 is the magnetic potential in region 1 and 2; M-⟶ is the magnetization strength of permanent magnet array roll; $\nabla\cdot\vec{M}$ is the dispersion of M-⟶.

In column coordinates, the magnetization intensity M can be expressed as:

$$\vec{M} = M_r\vec{e_r} + M_\theta\vec{e_\theta} + M_z\vec{e_z} \tag{19}$$

Where: M_r、M_θ、M_z are the r,θ,z direction magnetization intensity components.

The magnetisation intensity of the permanent magnet array rollers is observed to change discontinuously, but periodically. Through the Fourier transform, the magnetisation intensity component of the permanent magnet array roll is therefore:

$$\begin{aligned} &= \sum_{j=1}^{n}\sum_{i=1}^{n} f_r(i)f_r(j)\cos\frac{2i\pi z}{T_1}\cos\frac{2j\pi\theta}{T_2} \\ &= \sum_{j=1}^{n}\sum_{i=1}^{n} f_\theta(i)f_\theta(j)\cos\frac{2i\pi z}{T_1}\sin\frac{2j\pi\theta}{T_2} \\ &= \sum_{j=1}^{n}\sum_{i=1}^{n} f_z(i)f_z(j)\sin\frac{2i\pi z}{T_1}\cos\frac{2j\pi\theta}{T_2} \end{aligned} \tag{20}$$

$$\begin{aligned} f_r(i) &= \frac{2|\vec{M}|}{i\pi}\left(\sin\frac{i\pi L_1}{T_1} + \sin\frac{i\pi(L_1+2L_2)}{T_1}\right) \\ f_r(j) &= (1-\cos j\pi)\left(\frac{4}{2j\pi - T_2}\sin\frac{(2j\pi - T_2)\alpha_1}{2T_2}\right. \\ &\left. - \frac{4}{2j\pi + T_2}\sin\frac{(2j\pi + T_2)\alpha_1}{2T_2}\right)\sin\frac{j\pi(\alpha_1+\alpha_2)}{T_2} \\ &+2(1-\cos j\pi)\left(\frac{1}{2j\pi - T_2}\sin\frac{(2j\pi - T_2)\alpha_2}{2T_2} + \right. \\ &\left. \frac{1}{2j\pi + T_2}\sin\frac{(2j\pi + T_2)\alpha_2}{2T_2}\right) \end{aligned} \tag{21}$$

Preprints.org (www.preprints.org) | NOT PEER-REVIEWED | Posted: 5 July 2024 doi:10.20944/preprints202407.0466.v1

$$
\begin{aligned}
&= \frac{2|\bar{M}|}{i\pi}\left(\sin\frac{i\pi L_1}{T_1} + \sin\frac{i\pi(L_1+2L_2)}{T_1}\right)\\
f_\theta(j) &= (\cos j\pi - 1)\left(\frac{4}{2j\pi - T_2}\sin\frac{(2j\pi - T_2)\alpha_1}{2T_2}\right.\\
&\left. + \frac{4}{2j\pi + T_2}\sin\frac{(2j\pi + T_2)\alpha_1}{2T_2}\right)\sin\frac{j\pi(\alpha_1+\alpha_2)}{T_2}\\
&+2(\cos j\pi - 1)\left(\frac{1}{2j\pi - T_2}\sin\frac{(2j\pi - T_2)\alpha_2}{2T_2} - \right.\\
&\left.\frac{1}{2j\pi + T_2}\sin\frac{(2j\pi + T_2)\alpha_2}{2T_2}\right)
\end{aligned}
\tag{22}
$$

$$
\begin{cases}
f_z(i) = \dfrac{2|\vec{M}|}{i\pi}\cos\dfrac{2i\pi L_1}{2T_1}(1-\cos i\pi)\\[2ex]
f_z(j) = -\dfrac{4}{j\pi}\sin\dfrac{j\pi}{2}
\end{cases}
\tag{23}
$$

Where: i, j is a non-zero natural number;. $T_1 = 2L_1 + 2L_2$ 、 $T_2 = 4\alpha_1 + 2\alpha_2$

From Equation (18), we can get the magnetic potential φ1 and φ2, and then through Equation (16), we can get the solutions of the magnetic field strength H-→1 and H-→2 in the regions 1 and 2.

The special solutions of $\vec{H}_1$ and $\vec{H}_2$ can be determined from the boundary conditions of Equation (24) and the continuity theorem of magnetic flux in regions 1 and 2.

$$
\begin{cases}
\bar{H}_1|_{r=\infty} = 0\\
\bar{H}_1 = \bar{H}_2 + \bar{M}|_{r=R_2}\\
\bar{H}_{2\theta}|_{r=R_1} = 0
\end{cases}
\tag{24}
$$

In the formula, $\overrightarrow{H_1}, \overrightarrow{H_2}$ are the magnetic field strengths of regions 1 and 2; $\vec{M}$ is the magnetization strength of the permanent magnet array rollers.

5. Finite Element Analysis of New Permanent Magnet Array Roller

The CAE simulation tool is utilized to construct the magnetic rolls of the present study with 36 and 21 permanent magnets in circum-axial direction respectively, where R_1=80mm, R_2=110mm, $\alpha_1=\alpha_2$=10. and $L_1=L_2$=30mm.

Figure 7 illustrates the finite element simulation of the magnetic flux density mode of the magnetic roller at a distance of 115mm from the centre of the magnetic roller. Figure 8 depicts the single-cycle radial-circumferential flux density change rule at a distance of 115mm from the centre of the magnetic roller. The peak values of radial-circumferential flux density are 0. At a distance of 120mm from the centre of the magnetic roller, the single-cycle radial-circumferential flux density change rule is shown in Figure 9, with peak values of radial-circumferential flux density of 0.55T and 0.35T, respectively. The peak values of radial-peripheral magnetic flux density are 0.55T and 0.35T, respectively.

Preprints.org (www.preprints.org) | NOT PEER-REVIEWED | Posted: 5 July 2024 doi:10.20944/preprints202407.0466.v1

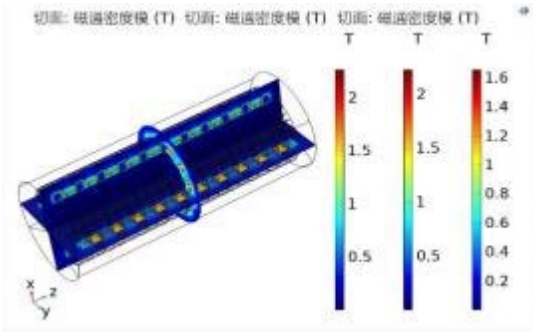

Figure 7. Flux density mode.

Figure 8. Radial and circumferential flux density.

ctionmay be

Figure 9. Radial and circumferential flux density.

divided by

The peak radial-peripheral flux densities of the Halbach array rolls at r=115mm from the roll centre are 0.62T and 0.70T for the same roll geometry and the same number of permanent magnets in the circumferential direction. For a given number of permanent magnets, the peak radial-peripheral flux density of the Halbach array roll is 0.62T and 0.70T at r=115mm, and the peak radial-peripheral flux density of the Halbach array roll is 0.44T and 0.45T at r=120mm from the roll centre. The axial flux density of the roller in this study is sinusoidal, with peaks and valleys of flux density that are stronger than those of the Halbach array roll. This results in a larger eddy current force during the separation process, which is more convenient for the separation of large-size crushed Cu-Al parts of scrap cars.

6. Conclusions

(1) A novel magnetic roller model with circum-axial periodic arrangement of permanent magnets is proposed. The mathematical model of the magnetic field of the magnetic roll is obtained by constructing the equivalent circulation model of a single permanent magnet and solving the system of magnetic scalar potential equations. The magnetic roll is optimised by changing the geometric parameter of the magnetic roll.

 doi:10.20944/preprints202407.0466.v1

(2) The axial arrangement of the new permanent magnet rolls is also periodic, which enhances the magnetic field strength and distance of the external magnetic field of the rolls, and generates greater eddy current force during the separation process, which is more conducive to the separation of large-size broken copper and aluminium parts of end-of-life automobiles.

Author Contributions: For research articles with several authors, a short paragraph specifying their individual contributions must be provided. The following statements should be used "Conceptualization, M.J. validation,Y.J.; formal analysis, L.W.; investigation, J.Z.; resources, J.L.; data curation, X.W.; writing—original draft preparation, Y.J.; writing—review and editing, Y.J.; supervision, J.L.; funding acquisition, S.Y. All authors have read and agreed to the published version of the manuscript." Please turn to the CRediT taxonomy for the term explanation. Authorship must be limited to those who have contributed substantially to the work reported.

Funding: This research was funded by National Natural Science Foundation of China (52065034), the Fundamental Research Funds for the Central Universities of China (N2303002) and The APC was funded by Kunming University of Science and Technology.

Institutional Review Board Statement: Not applicable.

Informed Consent Statement: Not applicable.

Conflicts of Interest: The authors declare no conflicts of interest.

References

1. ZHOU Xu, ZHU Shu-guang, CIXI La-mu, et al. Mechanical separation and recovery of spent lithiumion battery anode materials[J]. Transactions of Nonferrous Metals Society of China, 2011,21(12):3082-3086.
2. JIANG Ling, ZHAN Lu, ZHANG Qiu-zhuo. Separation and recovery of cobalt, nickel, manganese and lithium from acidic leaching solution of spent ternary battery positive active material[J].Transactions of Nonferrous Metals Society of China,2020,30(11):2684-2694.
3. GUO Miao-miao, XI Xiao-li, ZHANG Yun-he, et al. High temperature hydrogen reduction and hydrometallurgical recovery of valuable metals from spent nickel cobalt lithium manganate cathode materials for power batteries [J].Transactions of Nonferrous Metals Society of China, 2020,30(06):1415-1426.
4. YU Hai-jun, XIE Ying-hao, ZHANG Tong-zhu. Progress in recovery technology of vehicle power battery[J]. Trans- actions of Nonferrous Metals Society of China, 2014,24 (02):448-460.
5. LIU Jian-jun, LU Dong-fang, WANG Yu-hua, et al. Influence of dry magnetic separator on magnetite preconcen- tration under wind force[J]. Transactions of Nonferrous Metals Society of China,2020,30(10):2482-2491.
6. LU Dong-fang, WANG Yu-hua, HE Ping-bo,et al. Magneticfield simulation of crawler permanent magnet separator based on ANSYS[J]. Transactions of Nonferrous Metals Society of China, 2014,24(08):2188- 2194.
7. PAN Jian,ZHENG Guo-lin,ZHU De-qing,et al.Utilization of nickel slag using selective reduction followed by magnetic separation[J]. Transactions of Nonferrous Metals Society of China,2013,23(11).
8. CAO Yun-xiao, WANG Zhi-qiang, WANG Jin-jun, et al. Recovery of aluminum resources in fine-grained black aluminum ash based on particle dispersion and electric separation[J].Transactions of Nonferrous Metals Society of China,2019,29(05):1058-1064.
9. YANG Hui-fen,JING Li-li,DANG Chun-ge.Direct reduc- tion and magnetic separation recovery of iron in copper slag[J]. Transactions of Nonferrous Metals Society of China,2011,21(05):1165-1170.
10. KERCHER S A, WEBB M. Scrap processing by eddy current separation techniques[J].Resources and Conserv- ation,1982,8(1):61-74.
11. VANDERVALK H J L, BRAAM B C, DALMIJN W L. Eddy current separation by permanent magnets part I: theory[J].Resources and Conservation, 1986,12(1986): 233 -252.
12. FLETCHER D, GERBER R, LAWSON P,et al. Eddy curr- ent separation of nonferrous conductors and nonconduct- ors: theory and initial experiments [J]. IEEE Transactions on Magnetics,1991,27(6):5375-5377.
13. NORRGRAN D A,WERNHAM J A.Recycling and secon- dary recovery applications using an eddy-current separator [J].Minerals and Metallurgical Processing,1991,8(11):184 -187.
14. REM P C, LEEST P A,VANDENAKKER A J. A model for eddy current separation[J].International Journal Miner Pro- cessing,1997, 49(3):193- 200.
15. REM P C, BEUNDER E M,VANDENAKKER A J.Simula- tion of eddy-current separators[J]. IEEE Transactions on Magnetics, 1998, 34(4): 2280- 2286.
16. ZHANG Shun-li,FORSSBERG E,ARVIDSON B,et al. Alu- minum recovery from electronic scrap by High-Force® eddy current separators[J].Resources Conservation and Recycling,1998,23(4):225-241.

 doi:10.20944/preprints202407.0466.v1

17. ZHANG Shun-li,REM P C,FORSSBERG E.Particle traj- ectory simulation of two-drum eddy current separators[J]. Resources Conservation and Recycling,1999,26(1999):71 -90.
18. SCHLETT Z, LUNGU M. Eddy-current separator with inc-lined magneticdisc[J]. Minerals Engineering, 2002, 15(5): 365-367.
19. LUNGU M. Separation of small nonferrous particles using an angular rotary drum eddy-current separator with perma- nent magnets[J].IEEE Transactions on Magnetics,2005, 78(1): 22-30.
20. LUNGU M, REM P C. Eddy-current separation of small nonferrous particles by a single-disk separator with permanent magnets[J].IEEE Transactions on Magnetics, 2003, 39(4):2062-2067.
21. ROY S,ARI V,KONAR J,et al.Metal Enrichment of Finely Ground electronic waste using eddy current separation[J]. Separation Science and Technology, 2012, 47(12): 1777- 1784.
22. RAHMAN M A,BAKKER M C M. Sensor-based control in eddy current separation of incinerator bottom ash[J]. Waste Management, 2013, 33(6):1418-1424.
23. AMIR M,KARIM M, MOURAD B B,et al. Design and development of a low cost technique for sorting household wastes using eddy current separation process[J]. Interna- tional Journal of Environmental Studies, 2016, 73(2):203- 213.
24. WANG Quanqiang, DUAN Chenlong, ZHANG Hong jian. Study on the effect of eddy current operation parameters on aluminum separation[J]. Comprehensive utilization of resources in China,2005, 12:22-25.
25. RUAN Ju-jun,LI Jia,XU Zhen-ming.An environmental frie- ndly recovery production line of waste toner cartridges[J]. Journal of Hazardous Materials,2011,185(2):696-702.
26. YU Dun-song, LI Ming-bo, WANG Jun-chao, et al. Devel- opment status and prospect of eddy current separation of nonferrous metals from retired vehicles[J]. Material guide, 2015, 29 (03):59-67.
27. LI Jia,JIANG Yi-qun,XU Zhen-ming.Eddy current separ- ation technology for recycling printed circuit boards from crushed cellphones[J].Journal of Cleaner Production, 2016, 141 (2017):1316-1323.
28. LI Jian-bo, XU Zheng, JI Zhong-guang,et al. Research on separation and recovery process of waste lithium ion power battery based on regular crushing[J].Rare metals, 2019,43(07):746-753.
29. WEI Hong-gang,RAN Hong-xiang.Development of eddy current separator for recycling waste nonferrous metals and Research on conductor ejection trajectory[J].Nonferr- ous metals(mineral processing),2020(03):114-118+ 125.
30. YE Fang-ping,REN Xiang-jun,LIAO Guo-ping,et al.Ma- thematical model and experimental investigation for eddy current separation of nonferrous metals[J]. Results in Physics,2020,17(2020).
31. CHEN Da-lin,LIU Jian-xiong,GUO Sheng-hui,et al.Eddy current separation mechanism of thin-walled special- shaped copper aluminum parts of end-of-life vehicles [J]. Chinese Journal of non- ferrous metals,2020,30(06): 1406- 1414.
32. WANG Di, MA Xiu-shui, ZHI Xiong-fei, et al. Research review of scrap metals eddy current separation technology [J].Sensors and Transducers,2013,158(11): 242-248.